Enhanced caloric effect induced by magnetoelastic coupling in NiMnGaCu Heusler alloys: Experimental study and theoretical analysis

Dewei Zhao,[1,2] Teresa Castán,[3] Antoni Planes,[3] Zongbin Li,[4] Wen Sun,[1] and Jian Liu[1,2,*]

[1]*CAS Key Laboratory of Magnetic Materials and Devices, and Zhejiang Province Key Laboratory of Magnetic Materials and Application Technology, Ningbo Institute of Materials Technology and Engineering, Chinese Academy of Sciences, Ningbo 315201, China*

[2]*University of Chinese Academy of Sciences, 19 A Yuquan Road, Shijingshan District, Beijing 100049, People's Republic of China*

[3]*Departament de Física de la Matèria Condensada, Facultat de Física, Universitat de Barcelona, Diagonal 647, 08028 Barcelona, Catalonia, Spain*

[4]*Key Laboratory for Anisotropy and Texture of Materials (Ministry of Education), Northeastern University, Shenyang 110819, People's Republic of China*

(Received 9 October 2017; published 27 December 2017; corrected 22 January 2018)

On the basis of a phenomenological Landau model combined with comprehensive experimental studies, the magnetostructural transition behavior and field induced caloric effects for NiMnGaCu Heusler alloys have been investigated. In $Ni_{50}Mn_{25-x}Ga_{25}Cu_x$ alloys with $x = 5.5$, 6, and 6.5, both magnetocaloric entropy change (ΔS) and elastocaloric temperature change (ΔT) increase with the increment of Cu content. The maximum ΔS of 1.01 J/mol K and ΔT of 8.1 K are obtained for the alloy with $x = 6.5$. In order to explore the physical origin behind the large caloric effect, here we quantitatively propose a crucial coefficient of magnetoelastic coupling $\tilde{\kappa}$ by utilizing a thermodynamic formalism within the framework of the Landau approach. It has been verified that the enhancement of the strength of magnetoelastic coupling between lattice and magnetic freedoms results in the increased caloric response for NiMnGaCu alloys. Thus, the strengthened coupling of the magnetoelastic effect can be considered as an effective way to improve the caloric performance for these alloys having the same sign of magnetic and elastic entropy changes contributed to the total caloric effect.

DOI: 10.1103/PhysRevB.96.224105

I. INTRODUCTION

Caloric effect, namely, the thermal response of a solid to an external field, has attracted increasing attention owing to its potential application for ecofriendly room-temperature refrigeration [1–2]. Adiabatic temperature change (ΔT) and isothermal entropy change (ΔS) are generally used to quantify the caloric effect. Giant caloric effect is expected to exhibit in materials with first-order phase transformation [3–7]. The high latent heat output of field driven phase transformation gives rise to the large thermal response of the materials. In particular, multiferroic materials with more than one ferroic feature, such as ferromagnetic, ferroelastic, and ferroelectric properties, have received more interest [8]. Their phase transformation is capable to be induced by the fields conjugated to each ferroic property owing to the strong coupling effect between ferroic properties. Thus, various caloric effects including multicaloric effect are reported to be shown in such materials. NiMn-based metamagnetic shape memory alloys (SMAs) are known as an important class of magnetostructural multiferroics [9]. On cooling/heating, these alloys undergo the martensitic/austenitic transformation accompanied by a large change in magnetization. Due to the coupling effect of ferroelastic and ferromagnetic properties, magnetic field, uniaxial stress, and hydrostatic pressure induced phase transformation can be realized, resulting in the corresponding magnetocaloric, elastocaloric, and barocaloric effects [4,7,10–11].

In NiMn(In, Sn, Sb)-based metamagnetic SMAs, the austenite with a Heusler structure is ferromagnetic while the lower symmetric martensite is paramagnetic or antiferromagnetic [9,12–15]. The austenite shows a higher lattice vibration entropy due to the low-energy TA_2 phonons [16] but a lower magnetic entropy as compared to the martensite; i.e., the two subsystems, lattice and magnetism, contribute oppositely to the total ΔS during the phase transformation. Besides, more than half of the total ΔS stems from the lattice vibration entropy change [10–11]. Therefore, a common method to increase ΔS in these alloys is sacrificing the magnetic part by tuning the martensitic transformation close to the Curie transition of austenite [17–19]. However, the weakening of the magnetic part causes the loss of excellent coupling effect between ferroic properties. Thus, such a contradiction between enhancement of caloric response and excellent coupling effect has to limit the caloric performance of the alloys. In addition, the impacts of magnetic and mechanical fields on the phase stability are also conflicting. The magnetic field favors the ferromagnetic austenite while the application of the stress field would stabilize the martensite. This brings about a practical difficulty to markedly enhance the caloric performance through simultaneously applying multiple fields in these metamagnetic SMAs. In comparison, the other kind of alloys with low-magnetic austenite and high-magnetic martensite are highly desirable. In that case, the ferroelastic and ferromagnetic properties can be coupled positively and the above-mentioned contradictory points might be solved.

It is well known that the stoichiometric Ni_2MnGa alloy is a typical ferromagnetic SMA, which undergoes the martensitic transformation at 188 K and a Curie transition at 364 K [20]. The structural and magnetic transformations in Ni_2MnGa can be assumed to occur separately because the change in

*Corresponding author: Key Laboratory of Magnetic Materials and Devices, Ningbo Institute of Material Technology and Engineering, CAS, Ningbo 315201, China; liujian@nimte.ac.cn

magnetization during the martensitic transformation is very small. Previous studies show that substituting Mn with Cu in Ni_2MnGa can tune the martensitic transformation to a higher temperature and meanwhile decrease the Curie temperature (T_C) [20–22]. As a result, the structural and magnetic transformations are gradually coupled and a magnetostructural transformation from paramagnetic austenite to ferromagnetic martensite can be obtained in some special compositions. The influence of Cu can be explained by taking into account the change of electronic structure of the system [23]. On the one hand, doping Cu increases the delocalization of the Mn magnetism. The magnetism in the Cu-doped alloys is localized into the Mn atoms to less extent than that in Ni_2MnGa and it is expected that minority Mn spins interact with Ni spins to form a band. Thus, the magnetic interaction is weakened, giving rise to the decreases of the saturation magnetization and T_C. In addition, Cu substitution reinforces the Ni-Ga chemical bond. Due to the stronger Ni-Ga bonding, more energy is required to trigger the martensitic transformation, which results in an increase of martensitic transformation temperature (T_M). Actually, these results suggest that the martensite becomes more magnetically isotropic with doping Cu. With regard to the caloric effect of NiMnGaCu alloys, magnetocaloric effect for some compositions has been investigated and large values of ΔS associated with magnetic field induced phase transformation were reported in coupled alloys [22,24–25]. The origin behind the large caloric effect, however, has not been elucidated specifically. Additionally, there has been no report on the stress induced caloric effect in these alloys.

The interaction between the ferromagnetic and ferroelastic properties of materials is referred to as magnetoelastic coupling. The physical origin of the coupling effect is the dependence of magnetic exchange interaction on the distance between atomic magnetic moments [26]. In NiMn-based magnetic SMAs, the magnetic moments are mainly localized at Mn atoms and the exchange interaction between them is an oscillatory Ruderman-Kittel-Kasuya-Yosida type of coupling. The distance between Mn atoms significantly influences the magnetic behavior of these alloys [27–30]. Thus, the magnetoelastic coupling in NiMn-based alloys can be attributed to the strong sensitivity of the magnetic exchange interaction to the distance of Mn atoms. Recently, the present authors proposed a general thermodynamic framework to investigate the cross contribution arising from the magnetoelastic coupling to the caloric effect in multiferroic materials [31]. A corresponding relation between simulative magnetoelastic coupling parameters and (T_C - T_M) was built in NiMnInCo metamagnetic SMAs. The theoretical dependence of ΔS on (T_C - T_M) agreed well with the experimental data, indicating that the strength of magnetoelastic coupling can significantly influence the value of ΔS. In this paper, we present experimental data on magnetocaloric and elastocaloric effects in NiMnGaCu alloys, at the same time utilizing the established thermodynamic framework to quantitatively analyze the effect of magnetoelastic coupling on the caloric effect of these alloys. The experimental results show that the increment of Cu content enhances the caloric response, which originates from the strengthening of magnetoelastic interplay. Combining the theoretical and experimental studies, we conclude that caloric performance can be improved by strengthening the magnetoelastic coupling for this type of alloys with low-magnetic austenite and high-magnetic martensite.

II. EXPERIMENTAL DETAILS

$Ni_{50}Mn_{25-x}Ga_{25}Cu_x$ ($x = 1$, 2, 3, 4, 5, 5.5, 6, and 6.5, hereafter referred to as Cux) ingots were arc melted under an argon atmosphere. Textured polycrystalline rods of Cu5.5, Cu6, and Cu6.5 were grown by a liquid-metal-cooling directional solidification method with a given crystal growth rate of 150 μm/s [32]. The samples were homogenized at 1073 K for 24 h in a vacuum followed by quenching into ice water. Compressive samples with nominal size of $3 \times 3 \times 6\,mm^3$ were cut from the rods.

A Pyris Diamond differential scanning calorimeter (DSC) was used to characterize the phase transformation temperatures. The actual compositions were determined as $Ni_{50.0}Mn_{19.8}Ga_{24.7}Cu_{5.5}$ for Cu5.5, $Ni_{50.2}Mn_{19.1}Ga_{24.7}Cu_{6.0}$ for Cu6, and $Ni_{50.0}Mn_{19.0}Ga_{24.6}Cu_{6.4}$ for Cu6.5, by inductively coupled plasma-optical emission spectroscopy (PE Optima 2100DV). Crystal structure of NiMnGaCu alloys was identified by x-ray diffraction (XRD, Bruker D8) employing Cu-$K\alpha$ radiation. A superconducting quantum interference device (Quantum Design MPMS-5S) was used to analysis magnetic properties. Compression experiment by using the sample with a size of $3 \times 3 \times 6\,mm^3$ was performed on a universal testing machine equipped with a heating furnace. Isothermal and adiabatic compression conditions were established by setting the strain rates of 2.8×10^{-4} and $4.2 \times 10^{-2}\,s^{-1}$, respectively. The ΔT of the specimen upon rapid unloading was recorded by a T-type thermocouple with accuracy better than $\pm$ 0.1 K welded on the middle of the sample surface.

III. RESULTS AND DISCUSSION

A. Phase transformation and crystal structure

Figure 1 shows the experimental phase diagram for the $Ni_{50}Mn_{25-x}Ga_{25}Cu_x$ ($x = 0-7$) alloys. The phase transformation temperatures for the alloys are determined from the DSC measurement and also partially taken from the literature [20]. It is apparent that T_M increases whereas T_C

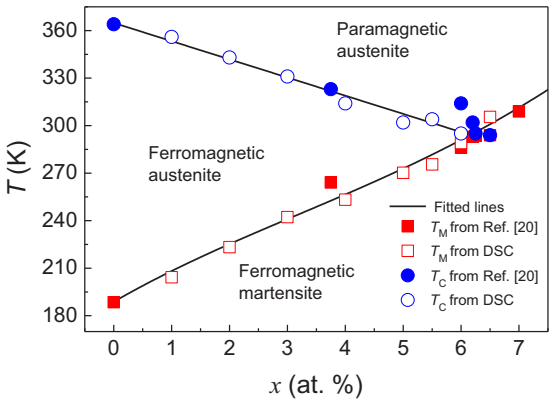

FIG. 1. Phase diagram for $Ni_{50}Mn_{25-x}Ga_{25}Cu_x$ ($x = 0-7$) alloys. Continuous lines denote the results of the model and symbols denote experimental data.

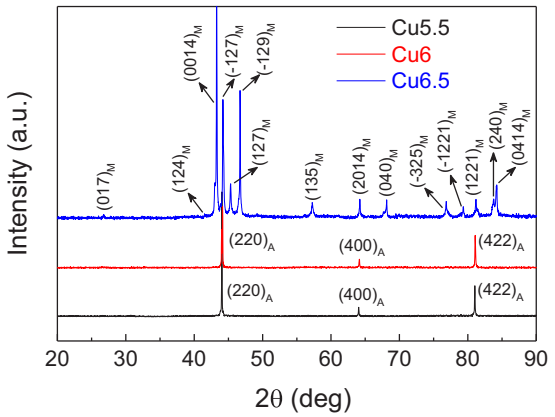

FIG. 2. XRD patterns for $Ni_{50}Mn_{25-x}Ga_{25}Cu_x$ ($x = 5.5$, 6, and 6.5) alloys at room temperature.

decreases with the Cu content. The dependence of T_C on x can be fitted to the equation (T_C in Kelvin and x in atomic percentage): $T_C(x) = 364.82 - 11.48x$. There exists a triple point in the phase diagram, at which the martensitic and magnetic transformations are coupled. The alloys with $x = 5.5$, 6, and 6.5 close to this triple point are selected for the following investigation.

Figure 2 shows the XRD patterns for Cux ($x = 5.5$, 6, and 6.5) alloys at room temperature. The patterns with $x = 5.5$ and 6 are indexed by a cubic austenitic structure with the lattice parameters $a_0 = 5.810$ and 5.804 Å, respectively, while the XRD pattern with $x = 6.5$ can be indexed as a $7M$ monoclinic martensitic structure and the lattice parameters are $a_M = 4.251$ Å, $b_M = 5.500$ Å, $c_M = 29.285$ Å, $\beta_M = 92.878°$.

The thermomagnetic curves for the alloys under a magnetic field of 500 Oe are shown in Fig. 3(a). For Cu5.5, the sudden increase upon cooling indicates the Curie transition of the austenite and the subsequent decrease corresponds to the martensitic transformation. Similar to Ni_2MnGa alloy, the magnetic and martensitic transformations are separated. The increase of Cu content shortens the interval between martensitic and Curie transformations. As a result, the two transformations are nearly coupled for Cu6, while the fully coupled magnetostructural transformation from paramagnetic austenite to ferromagnetic martensite takes place for Cu6.5. Using the extension method described in Ref. [33], the start (M_s and A_s) and finish (M_f and A_f) temperatures of martensitic and austenitic transformations and T_C for the alloys are determined, as listed in Table I. The thermal hysteresis defined as $\Delta T_{hys} = (A_s + A_f - M_s - M_f)/2$ is also listed. It should be noted that the hysteresis of the NiMnGaCu system is extremely small. Figure 3(b) shows the thermomagnetic curves under the magnetic field of 50 kOe. In all alloys, the magnetization of martensite is higher than that of austenite. The application of higher magnetic field increases the characteristic temperatures of martensitic transformation. It is worth noting that the difference in the magnetization (ΔM) between austenite and martensite as well as the shift of martensitic transformation temperature with magnetic field ($dT_M/d\mu_0 H$), as listed in Table I, increase with the Cu content. This is helpful to enhance the magnetoelastic interplay and realize the magnetic field induced martensitic transformation.

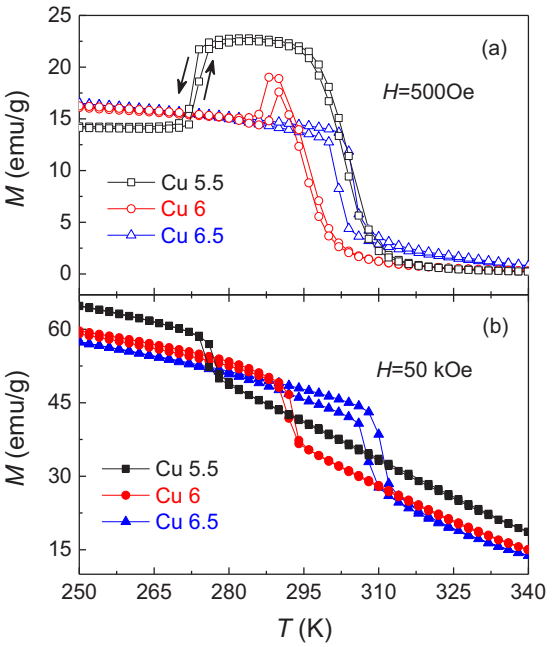

FIG. 3. Temperature dependence of magnetization for $Ni_{50}Mn_{25-x}Ga_{25}Cu_x$ ($x = 5.5$, 6, and 6.5) alloys at magnetic fields of 500 Oe (a) and 50 kOe (b). The arrows indicate the direction of temperature change.

B. Magnetocaloric effect

Magnetic field induced phase transformations for Cux ($x = 5.5$, 6, and 6.5) alloys are examined by continuously measuring isothermal magnetization curves with a cooling step of 2 K, as shown in Figs. 4(a)–4(c). A weak magnetic field induced martensitic transformation indicated by the sigmoidlike curve and magnetic hysteresis is observed in the curves at 273 and 275 K for Cu5.5 upon increasing the magnetic field. The magnetic field induced transformation for Cu6 and Cu6.5 alloys becomes more pronounced in a widened temperature interval due to the increase of ΔM and $dT_M/d\mu_0 H$. Magnetic entropy change (ΔS_m) can be obtained from integration of the Maxwell relation $(\frac{\partial S}{\partial H})_T = \mu_0 (\frac{\partial M}{\partial T})_H$ [34]:

$$\Delta S_m(T,H) = \mu_0 \int_0^H \left(\frac{\partial M(T,H)}{\partial T}\right)_H dH.$$

TABLE I. List of phase transformation parameters of $Ni_{50}Mn_{25-x}Ga_{25}Cu_x$ ($x = 5.5$, 6, 6.5) alloys determined from thermomagnetic curves: martensitic transformation start (M_s) and finish (M_f) temperatures, austenitic transformation start (A_s) and finish (A_f) temperatures, Curie temperature (T_C), thermal hysteresis (ΔT_{hys}), and magnetic field dependence of the martensitic transformation temperature ($dT_M/d\mu_0 H$).

x	M_s(K)	M_f(K)	A_s(K)	A_f(K)	T_C(K)	ΔT_{hys}(K)	$dT_M/d\mu_0 H$ (K/T)
5.5	275	271	272	276	304	1	0.6
6	288	286	288	290	295	2	0.8
6.5	304	300	303	307		3	1.2

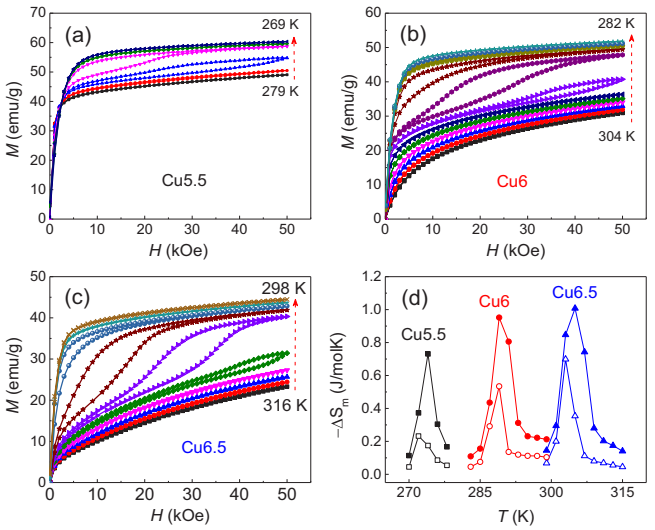

FIG. 4. Magnetization vs magnetic field curves at different temperatures with a cooling step of 2 K (a–c) and magnetic fields of 20 kOe (open symbols) and 50 kOe (solid symbols) induced entropy change as a function of temperature (d) for $Ni_{50}Mn_{25-x}Ga_{25}Cu_x$ ($x = 5.5$, 6, and 6.5) alloys.

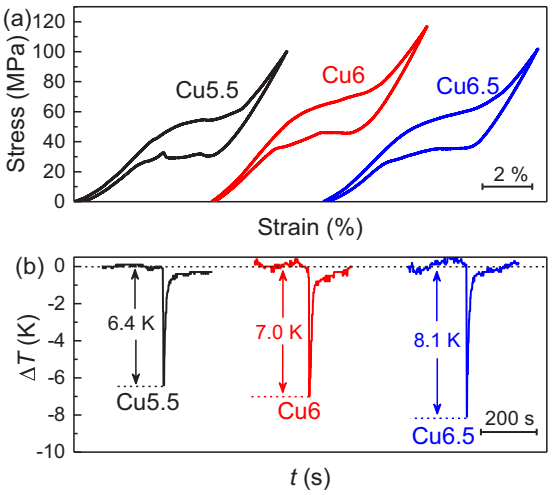

FIG. 5. (a) Stress-strain curves with a strain rate of 2.8×10^{-4} s^{-1} at 303 K for $Ni_{50}Mn_{19.5}Ga_{25}Cu_{5.5}$, at 310 K for $Ni_{50}Mn_{19}Ga_{25}Cu_6$, and at 315 K for $Ni_{50}Mn_{18.5}Ga_{25}Cu_{6.5}$ oriented samples. (b) Temperature-time profiles during rapid unloading with a strain rate of 4.2×10^{-2} s^{-1}.

The obtained ΔS_m as a function of temperature in the magnetic fields of 20 and 50 kOe are shown in Fig. 4(d). The negative sign of ΔS_m indicates that all alloys exhibit a conventional magnetocaloric effect. Besides, a peak can be seen in each curve and the peak value increases with magnetic field. In the magnetic field of 50 kOe, the maximum ΔS_m values are 0.73 J/mol K for Cu5.5, 0.95 J/mol K for Cu6, and 1.01 J/mol K for Cu6.5. It can be found that the increment of Cu content increases the transformation volume in a limited magnetic field and enhances the magnetocaloric performance of the alloys.

C. Elastocaloric effect

As multiferroic materials, the phase transformation of NiMnGaCu alloys can also be induced by stress field. Uniaxial stress induced transformation and related elastocaloric effect are investigated in this section. Figure 5(a) shows the isothermal stress-strain curves with a strain rate of 2.8×10^{-4} s^{-1} at 303 K for Cu5.5, 310 K for Cu6, and 315 K for Cu6.5. Compressive tests are performed on the oriented directionally solidified samples. The uniaxial stress induced reversible martensitic transformation represented by the stress plateaus and typical superelastic behavior are observed in all curves. The full transformations for three samples have completed below 120 MPa. The relatively low stress level is beneficial to obtain a large specific elastocaloric effect ($\Delta T/\Delta\sigma$). Elastocaloric ΔT is detected upon rapid unloading and the corresponding temperature-time profiles are shown in Fig. 5(b). Arising from the latent heat of austenitic transformation, large cooling effects with different ΔT are exhibited in the unloading processes. The cooling ΔT value for Cu5.5 (6.4 K) is slightly lower than the value for Cu6 (7.0 K) and a quite higher value (8.1 K) is acquired in Cu6.5 alloy. One can assume that the increased ΔT value for Cu6.5 is associated to the achievement of the coupling of magnetic and structural transformations. Also, the value of $\Delta T/\Delta\sigma$ for Cu6.5 is 0.16 K/MPa, which is higher than those for most elastocaloric materials [35].

D. Thermodynamic analysis

In this section, we will analyze the origin behind the increasing caloric effect with Cu content in NiMnGaCu alloys using the thermodynamic formulism within the framework of the Landau approach. Two order parameters, shear strain ε, determining the structural change at the martensitic transformation, and magnetization m, are used to acquire the Landau free energy. For the sake of simplicity, the order parameters are assumed to be one dimensional. The general form of the Landau free-energy density function of the alloys is

$$f(T,\varepsilon, m) = f_\varepsilon(T, \varepsilon) + f_m(T, m) + f_{\varepsilon-m}(\varepsilon, m), \quad (1)$$

where $f_\varepsilon(T, \varepsilon)$ and $f_m(T, m)$ correspond to the pure contributions associated with ferroelastic and ferromagnetic properties, and $f_{\varepsilon-m}(\varepsilon, m)$ is the cross contribution arising from their interplay. Considering the symmetry arguments, the Landau expansions of the pure elastic $f_\varepsilon(T, \varepsilon)$ and magnetic $f_m(T, m)$ terms are as follows:

$$f_\varepsilon(T, \varepsilon) = \frac{a_\varepsilon}{2}(T - T_\varepsilon)\varepsilon^2 - \frac{b}{4}\varepsilon^4 + \frac{c}{6}\varepsilon^6, \quad (2)$$

$$f_m(T, m) = \frac{a_m}{2}(T - T_c)m^2 + \frac{\beta}{4}m^4, \quad (3)$$

where T_ε is the low stability limit of the paraelastic phase and T_C is the ferromagnetic-paramagnetic transformation temperature. In the previous formulas, all parameters are positive constant and the minus sign before $\frac{b}{4}\varepsilon^4$ ensures the first-order nature of the structural transformation. The lowest-order Landau expansion for the coupling term allowed

by symmetry is

$$f_{\varepsilon-m}(\varepsilon, m) = -\mu\varepsilon m^2 - \kappa\varepsilon^2 m^2. \quad (4)$$

The first term is expected to be dominant near $x \approx 0$ and accounts for the large magnetocrystalline anisotropy induced by the martensitic transformation. The second coupling term should be dominant in the region in which the structural and magnetic transformations join each other. Since this is the region of interest here, from now on, we assume $\mu \approx 0$.

To account for the application of external fields, we define the following Gibbs free energy: $g(\sigma, h, T) = f(\varepsilon, m, T) - \sigma\varepsilon - hm$. This free energy can be rescaled by defining the following dimensionless quantities:

$$\tilde{g} = \frac{g}{b^3/c^2}, \quad \tilde{m} = \frac{m}{\left(\frac{a_m}{a_\varepsilon}\frac{b^2}{c\beta}\right)^{1/2}}, \quad \tilde{\varepsilon} = \frac{\varepsilon}{(b/c)^{1/2}},$$
$$\tilde{\kappa} = \frac{\kappa}{(\beta b)^{1/2}}, \quad T^* = \frac{T}{T_C},$$
$$\tilde{\sigma} = \frac{\sigma}{b^3/c^2}(b/c)^{1/2}, \quad \tilde{h} = \frac{h}{b^3/c^2}\left(\frac{a_m}{a_\varepsilon}\frac{b^2}{c\beta}\right)^{1/2}$$

with

$$T_C = \frac{b^2}{a_\varepsilon c}, \quad \text{and} \quad \frac{\beta}{b} = \left(\frac{a_m}{a_\varepsilon}\right)^2.$$

Note that the first condition imposes the same temperature scale for structural and magnetic degrees of freedom, while the second ensures that the corresponding energy scales are the same.

In the absence of external applied field the rescaled free energy is given by

$$\tilde{f} = \tfrac{1}{2}(T - T^*_\varepsilon)\tilde{\varepsilon}^2 - \tfrac{1}{4}\tilde{\varepsilon}^4 + \tfrac{1}{6}\tilde{\varepsilon}^6 + \tfrac{1}{2}(T^* - 1)\tilde{m}^2 + \tfrac{1}{4}\tilde{m}^4 - \tilde{\kappa}\tilde{\varepsilon}^2\tilde{m}^2. \quad (5)$$

Using the scaled free energy, all the calculations will be performed assuming that $T^*_\varepsilon = \frac{T_\varepsilon}{T_C} = \frac{1}{3}$, which is consistent with the ratio between martensitic transformation and Curie temperatures, $\frac{T_M}{T_C} \approx 0.51$, for the alloy with $x = 0$. Minimization of the rescaled free-energy function with respect to $\tilde{\varepsilon}$ and $\tilde{m}$ gives the following equations of state:

$$[(T^* - T^*_\varepsilon) - \tilde{\varepsilon}^2 + \tilde{\varepsilon}^4 - 2\tilde{\kappa}\tilde{m}^2]\tilde{\varepsilon} = 0, \quad (6)$$

and

$$[(T^* - 1) + \tilde{m}^2 - 2\tilde{\kappa}\tilde{\varepsilon}^2]\tilde{m} = 0. \quad (7)$$

For our samples with $T_C > T_\varepsilon$, there are three solutions for the equations:

(i) $\tilde{m} = 0$ and $\tilde{\varepsilon} = 0$ for $T^* \geqslant 1$;

(ii) $\tilde{m}^2 = -(T^* - 1)$ and $\tilde{\varepsilon} = 0$ for $T^*_M(\tilde{\kappa}) \leqslant T^* \leqslant 1$; and

(iii) $(T^* - T^*_\varepsilon) - \tilde{\varepsilon}^2 + \tilde{\varepsilon}^4 - 2\tilde{\kappa}\tilde{m}^2 = 0$ and $(T^* - 1) + \tilde{m}^2 - 2\tilde{\kappa}\tilde{\varepsilon}^2 = 0$ for $T^* \leqslant T^*_M(\tilde{\kappa})$,

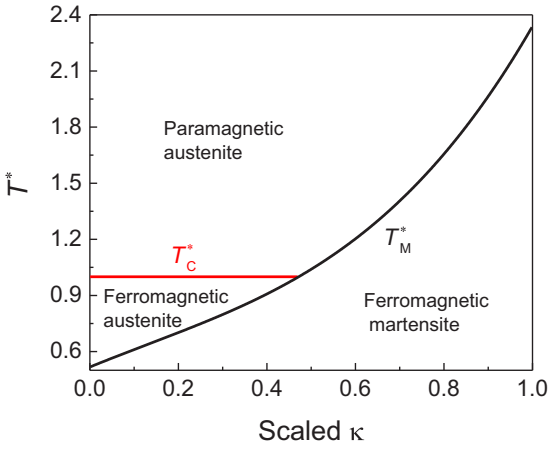

FIG. 6. Scaled magnetoelastic coupling coefficient dependence of scaled temperature T^*.

where $T^*_M(\tilde{\kappa})$ is the transition temperature for the paraelastic-ferroelastic transition. For solution iii, inserting $\tilde{m}^2 = 2\tilde{\kappa}\tilde{\varepsilon}^2 - (T^* - 1)$ into the expression of $\tilde{f}$, an effective free energy, $\tilde{f}_{\text{eff}}$, is gained:

$$\tilde{f}_{\text{eff}} = \tilde{f}_0(T^*) + \tfrac{1}{2}(1 + 2\tilde{\kappa})[T^* - T^*_\varepsilon(\tilde{\kappa})]\tilde{\varepsilon}^2 - \tfrac{1}{4}(1 + 4\tilde{\kappa}^2)\tilde{\varepsilon}^4 + \tfrac{1}{6}\tilde{\varepsilon}^6 \quad (8)$$

with $\tilde{f}_0(T^*) = -(T^* - 1)^2/4$. By requiring that the free energies of both ferroelastic and paraelastic phases are equal, one can obtain that $T^*_M(\tilde{\kappa}) = T^*_\varepsilon(\tilde{\kappa}) + \frac{3}{16}\frac{(1+4\tilde{\kappa}^2)^2}{1+2\tilde{\kappa}}$ with $T^*_\varepsilon(\tilde{\kappa}) = \frac{T^*_\varepsilon + 2\tilde{\kappa}}{1+2\tilde{\kappa}}$. Note that, as indicated before, $T^*_\varepsilon = \frac{T_\varepsilon}{T_C} = \frac{1}{3}$, which corresponds to $x = 0$. Figure 6 plots the phase diagram for the model. A triple point with $\tilde{\kappa}^* = 0.472$ is shown in the phase diagram. The behaviors of the order parameters above and below the triple point are different, as shown in Fig. 7. For $\tilde{\kappa} < \tilde{\kappa}^*$ ($\tilde{\kappa} = 0.20$), the model predicts two decoupled phase transformations corresponding to the continuous Curie transition at $T^* = 1$ and the discontinuous martensitic transformation at $T^* = T^*_M$. For the case of $\tilde{\kappa} \geqslant \tilde{\kappa}^*$ ($\tilde{\kappa} = 0.65$), a magnetostructural transformation from paramagnetic austenite to ferromagnetic martensite is shown.

In order to fit the model to the experimental phase diagram, the dependence of Curie temperature on x should be taken into account. According to the experimental data given in Sec. III A, the dependence is $T_C(x) = 364.82 - 11.48x$. x and $\tilde{\kappa}$ are related through

$$x = \frac{x^*}{\tilde{\kappa}^*}\tilde{\kappa} = \frac{6.163}{0.472}\tilde{\kappa}, \quad (9)$$

where $x^* = 6.163$ is the triple point of the experimental phase diagram, as shown in Fig. 1. This is equivalent to say that doping with Cu enhances the magnetoelastic interplay. Then, T^*_M should be also x dependent according to

$$T_M(x) = T^*_M T_C(x). \quad (10)$$

Finally, the fitted phase diagram is depicted in Fig. 1 as continuous lines. It is obvious that the resulting line of the model fits well with the experimental data.

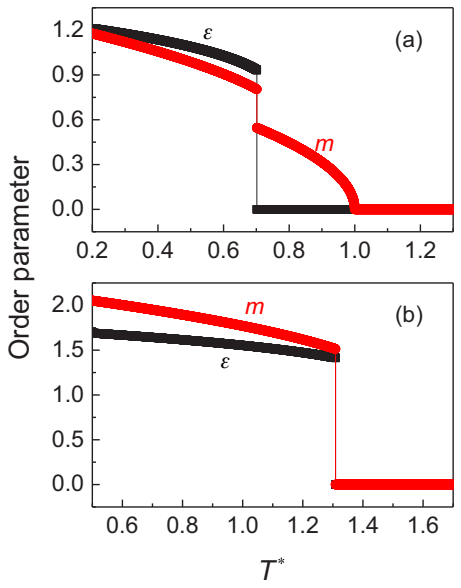

FIG. 7. Order parameters as a function of temperature for $\tilde{\kappa} = 0.20$ (a) and $\tilde{\kappa} = 0.65$ (b).

It should be noted that the scaled entropy change $\Delta\tilde{S} = \frac{c}{a_\varepsilon b}\Delta S$ at the martensitic transformation can also be calculated from Eq. (8) taking into account that $S = -\frac{\partial f}{\partial T}$. We obtain

$$\Delta\tilde{S} = \left(\frac{\partial \tilde{f}_{\text{eff}}}{\partial T}\right)_{\text{martensite}} - \left(\frac{\partial \tilde{f}_{\text{eff}}}{\partial T}\right)_{\text{austenite}} = \frac{1}{2}(1+2\tilde{\kappa})\left(\tilde{\varepsilon}_M^2 - \tilde{\varepsilon}_P^2\right) = \frac{3}{8}(1+2\tilde{\kappa})(1+4\tilde{\kappa}^2), \quad (11)$$

where $\tilde{\varepsilon}_M$ and $\tilde{\varepsilon}_P$ are the scaled structural order parameters of the coexisting martensitic and parent phases. Based on the equation, $\Delta\tilde{S} = \frac{3}{8}$ when $\tilde{\kappa} = 0$, i.e., $x = 0$. On the other hand, the experimental ΔS value for $x = 0$ is 0.28 J/mol K [20]. This leads to $\frac{a_\varepsilon b}{c} = 0.75$ J/mol K. Using this value, the theoretical ΔS as a function of x is computed. The theoretical results are shown in Fig. 8 and compared with the experimental data. The theoretical and experimental results are reasonably consistent and the value of ΔS increases with increasing x.

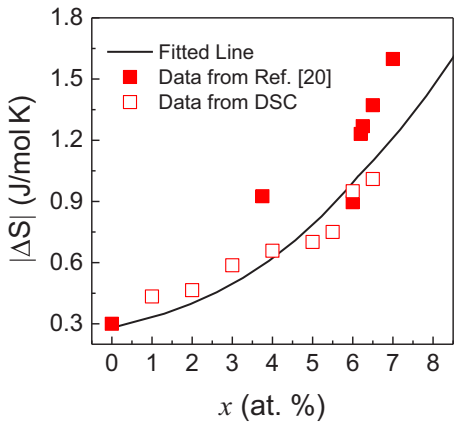

FIG. 8. $|\Delta S|$ as a function of x. Continuous lines denote the results of the model and symbols denote experimental data.

Based on the above, the proposed thermodynamic formulism simulates the phase diagram and ΔS at the phase transformation of $Ni_{50}Mn_{25-x}Ga_{25}Cu_x$ ($x = 0-7$) alloys commendably. Thus, the strength of magnetoelastic coupling can be quantitatively described by the rescaled coupling parameter $\tilde{\kappa}$. It can be found that the decoupled magnetic and martensitic transformations in Cu5.5 and Cu6 belong to the case of $\tilde{\kappa} < \tilde{\kappa}^*$, while the corresponding $\tilde{\kappa}$ value for the coupled Cu6.5 should be higher than the triple point $\tilde{\kappa}^*$. The enhancement of magnetoelastic interplay with Cu content results in an increase of ΔS at the phase transformation. Therefore, the increased magnetocaloric and elastocaloric responses with the Cu content in the present alloys can be doubtlessly attributed to the strengthening of magnetoelastic coupling. Besides, the present thermodynamic formulism can also be used in other magnetostructural multiferroics with positive magnetoelastic coupling to predict the entropy change on phase transformations.

IV. CONCLUSION

In summary, magnetocaloric and elastocaloric effects in $Ni_{50}Mn_{25-x}Ga_{25}Cu_x$ alloys with $x = 5.5$, 6, and 6.5 have been investigated experimentally. The results of magnetocaloric ΔS and elastocaloric ΔT with Cu content show that the maximum absolute values of ΔS and ΔT are 1.01 J/mol K and 8.1 K for Cu6.5 alloy, respectively. The physical origin behind the large caloric effect has been analyzed by taking the effect of magnetoelastic coupling on the ΔS at the phase transformation into account. Utilizing a thermodynamic formulism within the framework of the Landau approach, the strength of magnetoelastic coupling is quantitatively described by the rescaled coupling parameter $\tilde{\kappa}$. It has been verified that the enhancement of magnetoelastic interplay with Cu content results in a large ΔS. Thus, the increased caloric response with Cu content in alloys with $x = 5.5$, 6, and 6.5 can be attributed to the strengthening of magnetoelastic coupling. The theoretical and experimental results indicate that in a system with low magnetic austenite and high magnetic martensite strengthening the magnetoelastic interplay can effectively enhance the caloric performance of the alloys. Also, both the magnetic and stress fields favor the martensite with a higher magnetization, rendering these alloys suitable candidates for the investigation of multicaloric effect.

ACKNOWLEDGMENTS

The research leading to these results has received funding from the National Natural Science Foundation of China (Grants No. 51771218, No. 51531008, No. 51701233, and No. 51571056) and Zhejiang Provincial Natural Science Foundation of China (Grant No. LQ17E010004). T.C. and A.P. were supported by the Spanish Ministry of Economy and Competitiveness, Project No. MAT2016-75823-R.

[1] S. Fähler, U. K. Rößler, O. Kastner, J. Eckert, G. Eggeler, H. Emmerich, P. Entel, S. Müller, E. Quandt, and K. Albe, Adv. Eng. Mater. **14**, 10 (2012).

[2] L. Mañosa, A. Planes, and M. Acet, J. Mater. Chem. A **1**, 4925 (2013).

[3] V. K. Pecharsky and K. A. Gschneidner, Jr., Phys. Rev. Lett. **78**, 4494 (1997).

[4] T. Krenke, E. Duman, M. Acet, E. F. Wassermann, X. Moya, L. Mañosa, and A. Planes, Nat. Mater. **4**, 450 (2005).

[5] A. S. Mischenko, Q. Zhang, J. F. Scott, R. W. Whatmore, and N. D. Mathur, Science **311**, 1270 (2006).

[6] E. Bonnot, R. Romero, L. Mañosa, E. Vives, and A. Planes, Phys. Rev. Lett. **100**, 125901 (2008).

[7] L. Mañosa, D. González-Alonso, A. Planes, E. Bonnot, M. Barrio, J. L. Tamarit, S. Aksoy, and M. Acet, Nat. Mater. **9**, 478 (2010).

[8] X. Moya, S. Kar-Narayan, and N. D. Mathur, Nat. Mater. **13**, 439 (2014).

[9] R. Kainuma, Y. Imano, W. Ito, Y. Sutou, H. Morito, S. Okamoto, O. Kitakami, K. Oikawa, A. Fujita, T. Kanomata, and K. Ishida, Nature (London) **439**, 957 (2006).

[10] J. Liu, T. Gottschall, K. P. Skokov, J. D. Moore, and O. Gutfeisch, Nat. Mater. **11**, 620 (2012).

[11] B. F. Lu, F. Xiao, A. R. Yan, and J. Liu, Appl. Phys. Lett. **105**, 161905 (2014).

[12] K. Oikawa, W. Ito, Y. Imano, Y. Sutou, R. Kainuma, K. Ishida, S. Okamoto, O. Kitakami, and T. Kanomata, Appl. Phys. Lett. **88**, 122507 (2006).

[13] K. Koyama, K. Watanabe, T. Kanomata, R. Kainuma, K. Oikawa, and K. Ishida, Appl. Phys. Lett. **88**, 132505 (2006).

[14] R. Kainuma, Y. Imano, W. Ito, H. Morito, Y. Sutou, K. Oikawa, A. Fujita, K. Ishida, S. Okamoto, O. Kitakami, and T. Kanomata, Appl. Phys. Lett. **88**, 192513 (2006).

[15] J. Du, Q. Zheng, W. J. Ren, W. J. Feng, X. G. Liu, and Z. D. Zhang, J. Phys. D **40**, 5523 (2007).

[16] A. Planes and L. Mañosa, Solid State Phys. **55**, 159 (2001).

[17] W. Ito, Y. Imano, R. Kainuma, Y. Sutou, K. Oikawa, and K. Ishida, Metal. Mater. Trans. A **38**, 759 (2007).

[18] S. Kustov, M. L. Corró, J. Pons, and E. Cesari, Appl. Phys. Lett. **94**, 191901 (2009).

[19] V. Recarte, J. I. Pérez-Landazábal, V. Sánchez-Alarcos, V. Zablotskii, E. Cesari, and S. Kustov, Acta Mater. **60**, 3168 (2012).

[20] S. K. Sarkar, Sarita, P. D. Babu, A. Biswas, V. Siruguri, and M. Krishnan, J. Alloys Comp. **670**, 281 (2016).

[21] M. Kataoka, K. Endo, N. Kudo, T. Kanomata, H. Nishihara, T. Shishido, R. Y. Umetsu, M. Nagasako, and R. Kainuma, Phys. Rev. B **82**, 214423 (2010).

[22] Z. B. Li, N. F. Zou, C. F. Sánchez-Valdés, J. L. Sánchez Llamazares, B. Yang, Y. Hu, Y. D. Zhang, C. Esling, X. Zhao, and L. Zuo, J. Phys. D **49**, 025002 (2016).

[23] S. Roy, E. Blackburn, S. M. Valvidares, M. R. Fitzsimmons, S. C. Vogel, M. Khan, I. Dubenko, S. Stadler, N. Ali, S. K. Sinha, and J. B. Kortright, Phys. Rev. B. **79**, 235127 (2009).

[24] S. Stadler, M. Khan, J. Mitchell, N. Ali, A. M. Gomes, I. Dubenko, A. Y. Takeuchi, and A. P. Guimarães, Appl. Phys. Lett. **88**, 192511 (2006).

[25] V. Sokolovskiy, V. Buchelnikov, K. Skokov, O. Gutfleisch, D. Karpenkov, Yu. Koshkid'ko, H. Miki, I. Dubenko, N. Ali, S. Stadler, and V. Khovaylo, J. Appl. Phys. **114**, 183913 (2013).

[26] J. Evetts, *Concise Encyclopedia of Magnetic and Superconducting Materials* (Pergamon, New York, 1992), p. 766.

[27] V. D. Buchelnikov, P. Entel, S. V. Taskaev, V. V. Sokolovskiy, A. Hucht, M. Ogura, H. Akai, M. E. Gruner, and S. K. Nayak, Phys. Rev. B **78**, 184427 (2008).

[28] A. Planes, L. Mañosa, and M. Acet, Mater. Sci. Forum **738–739**, 391 (2013).

[29] R. B. Zhao, D. W. Zhao, G. K. Li, L. Ma, C. M. Zhen, D. L. Hou, W. H. Wang, E. K. Liu, J. L. Chen, and G. H. Wu, Appl. Phys. Lett. **105**, 232404 (2014).

[30] E. Şaşıoğlu, L. M. Sandratskii, and P. Bruno, Phys. Rev. B **77**, 064417 (2008).

[31] A. Planes, T. Castán, and A. Saxena, Phil. Trans. R. Soc. A **374**, 20150304 (2016).

[32] J. Liu, H. X. Zheng, Y. L. Huang, M. X. Xia, and J. G. Li, Scr. Mater. **53**, 29 (2005).

[33] A. Shen, D. W. Zhao, W. Sun, J. Liu, and C. J. Li, Scri. Mater. **127**, 1 (2017).

[34] A. M. Tishin, and Y. I. Spichkin, *The Magnetocaloric Effect and its Applications* (Institute of Physics, Bristol, 2003).

[35] Y. Li, D. W. Zhao, and J. Liu, Sci. Rep. **6**, 25500 (2016).